Large-scale Waves and Shocks in the Solar Corona

Alexander Warmuth

Astrophysikalisches Institut Potsdam, An der Sternwarte 16, D-14482 Potsdam, Germany
awarmuth@aip.de

Abstract. Large-scale waves and shocks in the solar corona are reviewed. The emphasis is on globally propagating wave-like disturbances that are observed in the low corona which have become known as "coronal transient waves" or "coronal Moreton waves". These phenomena have recently come back into focus prompted by the observation of wave-like perturbations in several spectral ranges, particularly in the extreme ultraviolet (with the *SOHO*/EIT instrument). The different observational signatures of coronal waves are discussed with the aim of providing a coherent physical explanation of the phenomena. In addition to imaging observations, radiospectral data are considered in order to point out the relation between coronal waves and metric type II radio bursts. Briefly, potential generation mechanisms of coronal waves are examined. Finally, the relevance of coronal waves to other areas of solar physics is reviewed.

1 Introduction

The solar corona is characterized by a magnetized plasma in which MHD waves and shocks can propagate. It is quite evident that a sudden disturbance of the medium – be it due to a solar flare or an eruption – will launch a wave. The first indications for such globally traveling disturbances were given by the activation of distant filaments by flares, first discussed by Dodson ([22]; see also [80]). Sympathetic flaring (in which a flare seems to trigger another flare in a distant active region) has also been claimed to provide evidence for traveling perturbations (e.g. [9, 104]), but the reality of this phenomenon has remained doubtful (cf. [11]).

Type II solar radio bursts [123], which are seen in dynamic radio spectra as narrow-band emission drifting from higher to lower frequencies, are interpreted as the signature of a collisionless fast-mode MHD shock [98] which expands through the corona and may even penetrate into the interplanetary space (e.g. [13]). The coronal type II bursts are called *metric type II bursts* because they are typically observed at meter wavelengths (for a review, see [4, 58]; see also Gopalswamy, this volume). Using a suitable coronal

A. Warmuth: *Large-scale Waves and Shocks in the Solar Corona*, Lect. Notes Phys. **725**, 107–138 (2007)
DOI 10.1007/978-3-540-71570-2_6

electron density model (e.g. [61, 72]), one can calculate the speed of the type II source, which typically lies around 1 000 km s^{-1}.

Large-scale propagating disturbances were finally directly imaged in 1960 using Hα filtergrams [3, 65, 66]. These disturbances, which have since become known as *Moreton waves* or *flare waves*, appear as arc-shaped fronts propagating away from flaring active regions (ARs) at speeds of the order of 1 000 km s^{-1}. The fronts are seen in emission in the center and in the blue wing of the Hα line, whereas in the red wing they appear in absorption. This is interpreted as a depression of the chromosphere by an invisible agent [67]. It was also shown that these waves can indeed cause the activation or "winking" of filaments [80].

Uchida [99] developed the theory that Moreton waves are just the "ground track" of a flare-produced fast-mode MHD wavefront which is coronal in nature and sweeps over the chromosphere ("sweeping-skirt hypothesis"). In numerical simulations, Uchida ([100]; see also [101]) was able to show how the waves become focused towards regions of low Alfvén velocity, producing wavefronts that agreed reasonably well with the observations. This model, also known as the blast-wave scenario, can also explain the type II bursts, which are generated at locations where the wavefront steepens to a shock [102]. The association of Moreton waves and type II bursts was also suggested by observations (e.g. [39]).

Since the 1970s, the blast wave scenario has been contested by an alternative model which postulated that coronal shocks are driven by coronal mass ejections (CMEs) acting as a piston (e.g. [17] and references therein). However, this discussion was mainly focused on type II bursts and interplanetary shocks, whereas comparatively little work was done on Moreton waves. This situation was reversed in 1997, when globally propagating wave-like features were detected in the low corona [92] with the Extreme Ultraviolet Imaging Telescope (EIT) aboard the Solar and Heliospheric Observatory (*SOHO*) spacecraft. Since then, wave features have been discovered in several additional spectral ranges. Whether all these signatures are created by the same mechanism is currently intensively debated.

Figure 1 illustrates the different coronal disturbances that can be generated by a solar eruption within the framework of the magnetic reconnection scenario. Reconnection occurs in the diffusion region (DR) below an erupting flux rope (which in this case contains an eruptive prominence – EP). Two pairs of slow-mode standing shocks (SMSS) expand outward from DR, bounding the hot outflowing jets. If the downflow jet is supermagnetosonic a fast-mode standing shock (FMSS; see [6]) is formed above the postflare loops (PFL).

In addition to these standing shocks, propagating waves and/or shocks may be launched. As the erupting flux rope develops into a CME, it can drive a shock provided it is fast enough. This type of shock can reach the outer corona and the heliosphere. The coronal shocks which produce metric type II bursts, on the other hand, may either be launched by the CME or by the flare. At last, there are the large-scale coronal waves which are observed

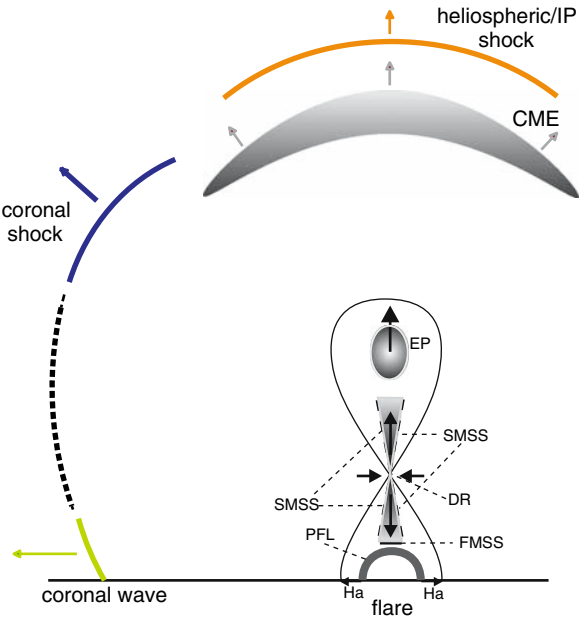

Fig. 1. Schematic representation of the coronal disturbances caused by a solar eruption. For details see main text (adapted from [6])

propagating along the solar surface. They are possibly connected with coronal shocks (indicated by the dashed curve), but it is still far from clear exactly in which manner the different phenomena are related.

In this review, I will focus on the last phenomenon mentioned: the large-scale, globally propagating *coronal waves* (also known as "coronal transient waves" or "coronal Moreton waves"). The basic physics relevant to these phenomena is briefly discussed in Sect. 2. The different observational signatures of the waves are summarized in Sect. 3, while their relation to metric type II bursts is discussed in Sect. 4. Possible physical interpretations of coronal waves are examined in Sect. 5. Potential generation mechanisms of coronal waves are discussed in Sect. 6, and the relevance of coronal waves to other areas of solar physics is reviewed in Sect. 7. The conclusions are given in Sect. 8.

2 The Physics of MHD Waves and Shocks

The solar corona is characterized by a magnetized plasma, which means that disturbances of the medium cannot be treated as purely hydrodynamic. Instead, we have to consider MHD waves and shocks. There are three characteristic MHD wave modes: *Alfvén*, *fast-mode* and *slow-mode* waves. In the

case of Alfvén waves, the magnetic tension acts as the restoring force ("shear Alfvén waves"). These waves propagate with $v = v_A cos\theta_B$, where θ_B is the inclination between the wave vector and the magnetic field, v_A the Alfvén speed

$$v_A = \frac{B}{\sqrt{4\pi\bar{\mu}m_p n}} , \tag{1}$$

where B is the magnetic field strength, $\bar{\mu}$ the mean molecular weight (taken as $\bar{\mu} = 0.6$ according to [79]), m_p the proton mass, and n the total particle number density.

For fast- and slow-mode waves, both the magnetic and the gas pressure act as restoring forces ("hybrid waves"). Their speed is

$$v_{fm/sm} = (\frac{1}{2}\left\{ v_A^2 + c_s^2 \pm \sqrt{(v_A^2 + c_s^2)^2 - 4v_A^2 c_s^2 \cos^2\theta_B} \right\})^{1/2} , \tag{2}$$

where c_s is the sound speed. The plus sign gives the fast-mode speed v_{fm}, while using the minus sign yields the slow-mode speed v_{sm}. Another important characteristic speed is the magnetosonic speed

$$v_{ms} = (v_A^2 + c_s^2)^{1/2} \tag{3}$$

which is the fast-mode speed for $\theta_B = 90°$. For an arbitrary inclination towards $\boldsymbol{B}$, v_{ms} gives an upper limit for v_{fm}, while v_A or c_s, whichever is greater, is the lower limit (for $\theta_B = 0°$). In many cases v_{ms} is used instead of v_{fm} because θ_B is not known. In the particular case of coronal waves, this is reasonable since they propagate along the solar surface where the magnetic field is predominantly radial.

An important parameter with regard to the propagation of MHD waves and shocks is the ratio of the magnetic pressure to the gas pressure, the so-called plasma beta

$$\beta_p = \frac{8\pi n k_B T}{B^2} = \frac{6c_s^2}{5v_A^2} , \tag{4}$$

where k_B is the Boltzmann constant and an adiabatic exponent of $\gamma = 5/3$ has been assumed. In most parts of the corona, $\beta_p \ll 1$, which implies also $v_A \gg c_s$. In that case, $v_{ms} = v_A$ can be assumed (i.e., the fast-mode wave has reduced to a compressional Alfvén wave).

So far we have discussed linear waves, which result for linear governing equations. This is an approximation since the basic MHD equations are inherently nonlinear. If a compressive MHD wave has a large amplitude, the nonlinear terms become important and lead to a steepening of the wave's profile. This can be visualized in the following manner: the crest of the wave moves faster than the characteristic velocity of the ambient medium because this speed is locally increased due to the compression. At the same time the leading and trailing edge of the wave still propagate with the ambient characteristic velocity. As a result the wave steepens as shown in Fig. 2. Such

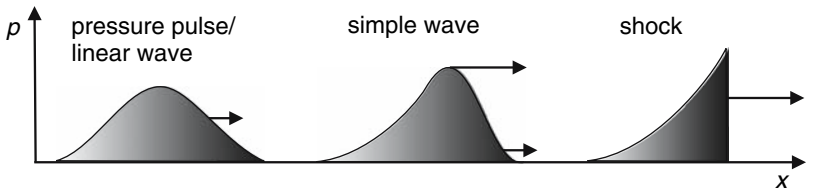

Fig. 2. Schematic of a freely propagating pressure disturbance in the solar corona (pressure p is shown as a function of distance x). An initial pressure pulse (*left*) propagates through the corona as a large-amplitude simple wave (*middle*). The perturbation profile steepens because the wave crest propagates faster than at the leading or trailing edge (*indicated by arrows*). The steepening may lead to the formation of a shock (*right*)

nonlinear large-amplitude waves are called *simple waves* [44, 54]. In the context of this review, we will focus on fast-mode simple waves [59].

Another possibility of a disturbance moving faster than the characteristic velocity of the medium is a *shock wave*. Both fast-mode and slow-mode nonlinear MHD waves can form shocks. A shock is a discontinuity at which the so-called Rankine-Hugoniot or jump conditions have to be fulfilled (see e.g. [79]). Fast-mode and slow-mode shocks are compressive – the downstream density is higher than the upstream one ($\rho_d > \rho_u$). For fast shocks, the downstream magnetic field component parallel to the shock surface increases as compared to the upstream one ($B_d > B_u$), while the converse is true for slow-mode shocks ($B_d < B_u$). Shock speeds can be given in terms of their Mach number, i.e. the Alfvénic Mach number $M_A = v_{shock}/v_A$ or the magnetosonic Mach number $M_{ms} = v_{shock}/v_{ms}$ (note that this nomenclature can also be used for simple waves).

Shocks can also be classified with regard to how they are generated. There are two main types: freely propagating shocks (also called blast-type) and driven shocks. *Freely propagating shocks* start as a large-amplitude disturbance of the medium, which propagates as a non-linear simple wave. The perturbation profile steepens until finally a discontinuity is formed (e.g. [106]) – a shock has been generated (see Fig. 2). As the shock propagates, its amplitude will drop due to geometric expansion, dissipation and the widening of the perturbation profile (the shocked edge moves faster than the trailing one). Ultimately, the shock will decay to an ordinary (i.e. small-amplitude) wave.

In contrast to the blast-type shocks, *driven shocks* are constantly supplied with energy by a driver or piston. There are two subtypes of driven shocks (see Fig. 3) that are often confused. In the true *piston shock* scenario, the medium is confined and cannot stream around the piston. In this geometry, the shock can move faster than the piston, and indeed a shock will be generated even if the piston moves slower than the characteristic speed of the medium. A spherical explosion is another example for such a scenario. In contrast to

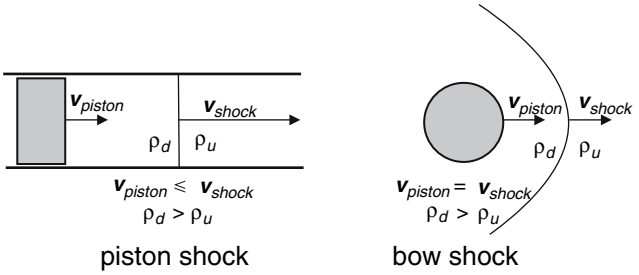

Fig. 3. Schematic of a piston-driven shock (*left*) and a bow shock (*right*)

that, a *bow shock* will form when the medium can stream around and behind the piston. In this case, the shock moves at the same speed as the piston. Moreover, a shock will only form if the piston is faster than the characteristic speed. The best example for this type of shock is the bow shock ahead of Earth's magnetosphere (see Burgess, this volume).

3 Signatures of Coronal Waves

We will now discuss the various observational signatures of coronal waves and their basic characteristics. Unless stated otherwise, the results given in this section are taken from [118].

3.1 Hα (Moreton Waves)

Moreton waves remain the best-studied signature of coronal waves because they have been observed for a long time (e.g. [66]) and because Hα data typically have a much higher time cadence than actual coronal images. A Moreton wave appears as an arc-like front (with an angular width of $\approx 100°$) at some distance from a flaring AR (≈ 100 Mm from the center of the flare). The leading edges of the earliest wavefronts agree very closely with a circular curvature. The front is bright in the line center and in the blue wing of Hα, while it is dark in the red wing. This is interpreted as a depression of the chromosphere by an invisible agent [67]. In the line wings one also sees a fainter front following the first one, where the signature of the intensity change in the wings is reversed as compared to the first front (thus dark in the blue wing and bright in the red wing). This front corresponds to the relaxation of the compressed chromosphere which expands upwards again. The velocity amplitude of the downward swing is some 6 - 10 $\mathrm{km\,s^{-1}}$ [91].

The Doppler shift strongly suggests that the Moreton wave appears only as a reaction to something pressing down from the corona and not due to a wave actually propagating in the chromosphere. This idea is supported by the observed speeds of Moreton waves: for a sample of 15 waves [88] have derived a

mean speed of $\langle v_{H\alpha} \rangle = 660$ km s^{-1}, and some Moreton waves reportedly have speeds above 1 000 km s^{-1}. However, in the chromosphere the characteristic velocities (e.g. sound speed c_s and Alfvén speed v_A) are of the order of tens of km s^{-1}. If Moreton waves were actually propagating *in* the chromosphere, they would have Mach numbers in excess of 10. Consequently they would suffer strong dissipation and would never propagate over larger distances.

As a Moreton wave moves away from the flare, it becomes increasingly fainter, diffuse and irregular, until its propagation can no longer be tracked. This is the case at distances of $\approx$300 Mm from the flare. An example of the typical evolution is shown in Fig. 4. The signs of decay are also present in the line wings. At the same time, the thickness of the wavefronts becomes larger. All this suggests that the coronal influence to which the chromosphere reacts becomes weaker and less coherent.

A new finding was that Moreton waves are not moving at a constant speed but decelerating [117]. With a sample of 12 events, [118] found an initial Moreton wave speed of $\langle v_1 \rangle = 845 \pm 162$ km s^{-1} (determined from the first wavefront pairs), but an average velocity (obtained from a linear fit) of $\langle \bar{v} \rangle = 643 \pm 179$ km s^{-1}, which agrees closely with the results of [88]. Evidently, Smith & Harvey were using linear fits and did not detect the deceleration. The kinematics of Moreton waves is thus better represented by a 2^{nd} degree polynomial fit. The mean deceleration obtained with this fit, averaged over the 12 waves, is $\langle \bar{a} \rangle = -1\,495 \pm 1\,262$ m s^{-2}. The waves do not display a constant deceleration, instead, the deceleration tends to become weaker with increasing time and distance. For example, if only the first three fronts are used to derive the polynomial fits, then the mean of all decelerations is significantly larger at $\langle \bar{a} \rangle = -2\,460$ m s^{-2}. Thus a power-law fit of the kinematical curves might be even more appropriate. The corresponding power-law index is $\langle \delta \rangle = 0.62 \pm 0.22$.

Moreton waves avoid strong concentrations of magnetic fields, such as ARs. This behavior could be reproduced by the coronal blast wave model of [100], who showed that a coronal fast-mode wave is refracted away from regions of high v_A, i.e. high magnetic field strength.

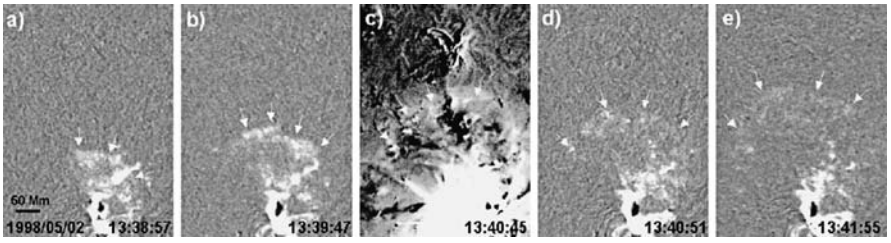

Fig. 4. Evolution of the Moreton wave of 1998 May 2 as shown by Hα (**a**, **b**, **d**, **e**; observed at Kanzelhöhe Solar Observatory) and EIT 195 Å (**c**) difference images. The wavefronts are indicated by *arrows* (from [118])

3.2 Extreme Ultraviolet (EIT Waves)

The Extreme Ultraviolet Imaging Telescope (EIT; see [19]) aboard the Solar and Heliospheric Observatory (*SOHO*) spacecraft has observed globally propagating wave-like disturbances in the corona since 1997 [92, 93]. These so-called *EIT waves* show a wide range of morphological patterns (cf. [49]). Usually they are observed as diffuse and irregular arcs of increased coronal emission in the 195 Å channel of EIT (centered on the Fe XII line, which corresponds to a plasma temperature of ≈ 1.5 MK). Figure 5 shows an example of a strong globally propagating EIT wave.

Limb observations of EIT waves clearly show that they can extend over a significant height range in the low corona, say ≈ 100 Mm. Sometimes EIT waves can be followed across the whole solar disk, which means that they can be tracked to much larger distances than Moreton waves. Note that waves in the EUV have also been observed by the *TRACE* satellite ([124]; see [35], for a description of the instrument).

EIT waves expand away from the site of AR transients (flares, CMEs) at speeds of a few 100 km s^{-1}. This seems to be at odds with the interpretation of EIT waves as the coronal counterpart of Moreton waves, which are on average 2–3 times faster. On the other hand, EIT waves also avoid concentrations of magnetic fields, but they may trigger transverse oscillations of AR loops [124] and filaments [75].

EIT waves are a relatively frequent phenomenon: from 1997 March to 1998 June 173 EIT waves were observed [12]. For comparison, Moreton waves occur roughly an order of magnitude less frequently. Interestingly, about 7% of the events in this big sample display sharp and bright wavefronts somewhat reminiscent of Moreton waves (e.g. [94]) – the so-called "brow waves" [31] or "S-waves" [12]. Such sharp wavefronts are only observed comparatively close to the source AR, and for or several S-waves (cf. Fig. 4) it was shown that they coincide spatially with Moreton waves observed at the same time [47, 118].

This would imply that at least S-waves are the long-sought coronal counterpart to Moreton waves, but what about the more common diffuse EIT waves? Most events showing S-waves also display diffuse fronts at a later

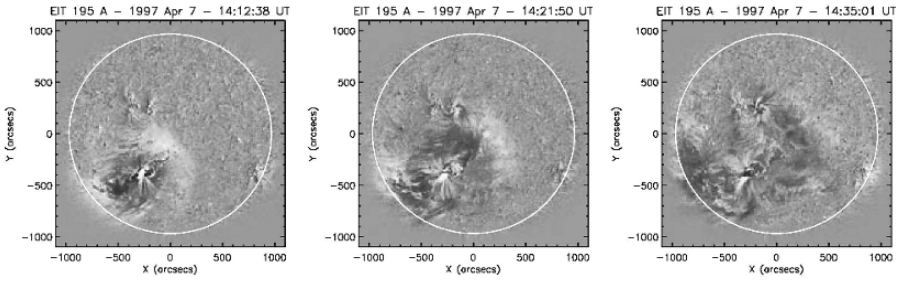

Fig. 5. *SOHO*/EIT 195 Å running difference images showing the globally propagating EIT wave of 1997 April 7

stage, which would be consistent with the idea of a decaying perturbation (see Sect. 3.1). Warmuth et al. [117] have shown that both the sharp and the diffuse EIT wavefronts can be produced by the same disturbance that creates the Moreton waves provided that this disturbance is decelerating (see the distance-time diagram in Fig. 6). The Moreton wave can only be observed relatively near to the source AR where it is still fast. In contrast, the low image cadence of EIT (≈ 15 min) combined with the fact that the waves can be traced to large distances in the EUV means that EIT samples the coronal disturbances when they have already propagated farther away and have thus already decelerated. In this scenario, EIT waves *must* have a lower average speed than Moreton waves. In a systematic study it could be shown that in eight Moreton/EIT wave events this deceleration scenario fits the observations [118]. Other authors (e.g. [23, 75]) have presented events where it is claimed that the two phenomena are distinct. It seems that observations with a higher temporal cadence than EIT will be required in order to positively resolve this issue. Note however that at least deceleration seems to be a characteristic of coronal waves in general, since there are also decelerating EIT waves without associated Moreton waves.

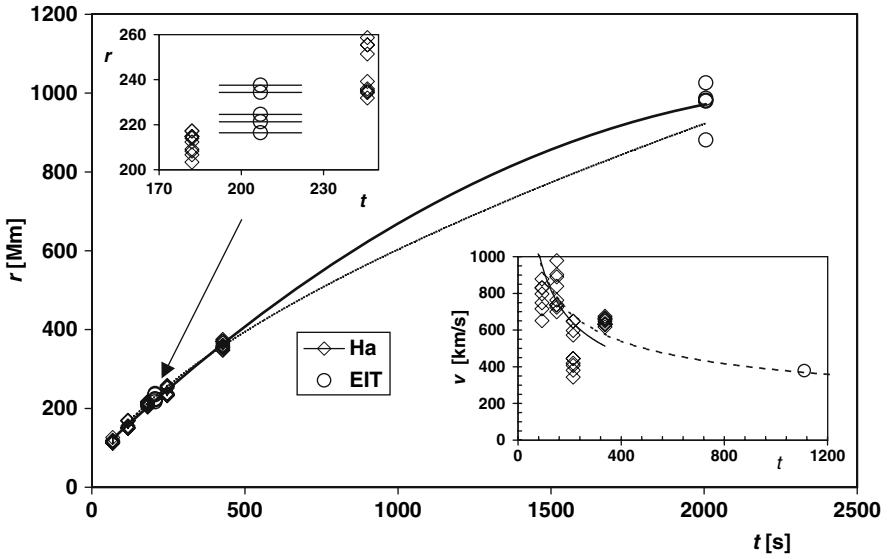

Fig. 6. The combined kinematics of the Moreton (*diamonds*) and EIT wavefronts (*circles*) in the event of 1998 May 2. The main plot shows distance r versus time t. In the upper inset an enlarged part of the graph shows the close association of the Hα and EIT fronts. Error bars are included for the EIT times. 2^{nd} degree polynomial (*thick line*) and power-law (*thin line*) fits are shown. The lower inset shows the velocities of the Moreton wave and the EIT wave. The *thick line* is a fit through the Hα $v(t)$ points, the *thin line* is the derivative of $r(t)$ shown in the main graph (after [117])

Many EIT waves are associated with *coronal dimming* which means a decrease of EUV emission in certain locations in the corona (e.g. [30, 46]). The dimming areas are rather inhomogeneous and can be quite complex. It is now accepted that coronal dimming is usually a result of a mass loss of emitting material, and not primarily due to a temperature change (e.g. [36, 38, 126]). As dimming is generally associated with CMEs, which are in turn often associated with EIT waves, it is well possible that the dimming in wave events is due to an associated CME [129] and not due to the waves themselves.

3.3 Soft X-rays

The observation of coronal waves in the EUV with *SOHO*/EIT came as a surprise since the Soft X-ray Telescope (SXT; see [97]) aboard *Yohkoh* had not observed such phenomena. This can be explained by the observation scheme used by SXT: a flare triggers a special observation mode which minimizes the field of view and the exposure time. These are not favorable conditions for the detection of coronal waves (for details, see [41]).

SXT has finally managed to observe a few coronal waves (see Fig. 7 for an example). Like EIT waves the disturbances observed with SXT show up as fronts of increased coronal emission. Morphologically, they are more homogeneous and generally "sharper" than EIT waves, and in this respect they more closely resemble Moreton waves. This is due to the fact that they are observed close to the source, whereas EIT waves are typically observed only farther out where the disturbance has already weakened and started to disintegrate.

Using a filter-ratio technique, [70] estimated a magnetosonic Mach number of 1.1–1.3 for a SXT wave under the assumption that it is a fast-mode MHD wave. For another SXT wave, [41] derived a comparable Mach number, an electron temperature in the range of 2–4 MK and an emission measure of 5×10^{26} cm^{-5}. An interesting feature of this event was that the wave was seen propagating along the solar limb: it reached a height of up to ≈ 100 Mm and became increasingly tilted towards the solar surface. This is consistent with refraction in a coronal model with v_A increasing with height [62, 99, 120].

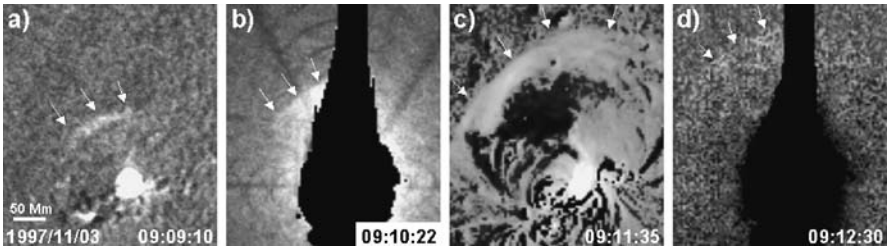

Fig. 7. The SXT wave of 1997 November 3 (**b**, **d**). The black features in the SXT images are artifacts of saturation. Additionally, the associated Moreton (**a**) and EIT wavefronts (**c**) are shown (from [118])

Since SXT waves are observed relatively close to the source AR, they can be compared to Moreton waves. In all SXT wave events that also had Hα coverage, corresponding Moreton wavefronts were observed (see Fig. 7). It was found that the wavefronts in both wavelength ranges are consistent with a common disturbance [47, 70]. Thus the waves seen in the SXR are really the coronal counterpart to Moreton waves.

Recently, Warmuth et al. [121] have observed global coronal waves with the Solar X-Ray Imager (SXI; see [40, 77]) aboard the *GOES*-12 satellite. Thanks to its cadence (2–4 min) SXI provides a link between the Moreton waves observed close to the AR and the remote EIT fronts. For six events, it could be shown that the wave features seen with SXI are decelerating and agree both with the Hα as well as with the EIT fronts (see Fig. 8 for an example). This is consistent with a single physical disturbance creating all wave signatures.

3.4 Helium I

The Helium I line at 10 830 Å (He I) is formed in a complicated manner (cf. [1]), with influences from the corona, transition region, and chromosphere. Simply put, absorption in the Helium I line increases with increasing UV and EUV flux from the corona and/or with an increase of collisional processes (due to a rise in temperature or density) in the transition region.

Wave signatures were detected in He I [25, 26, 111] with the CHIP instrument [56] at Mauna Loa Solar Observatory. These He I waves are seen in increased absorption. They are more diffuse and thicker than Moreton waves, and have a patchy structure that corresponds with the photospheric magnetic field and the chromospheric network (see Fig. 9 for an example). Some regions behind the He I front show a brightening which coincides with the locations of coronal dimming in cotemporal EIT images [111] observed behind EIT waves.

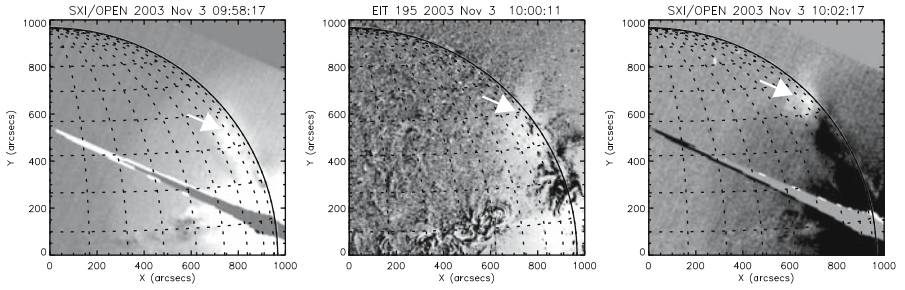

Fig. 8. The propagation of the coronal wave of 2003 November 3 as shown by SXI/OPEN (*left*, *right*) and EIT 195 Å (*middle*) running difference images. The wave is indicated by *arrows*. Note that the morphology of the wavefront is similar in SXR and EUV. The inclined linear feature in the SXI images is due to overexposure from the flare (from [121])

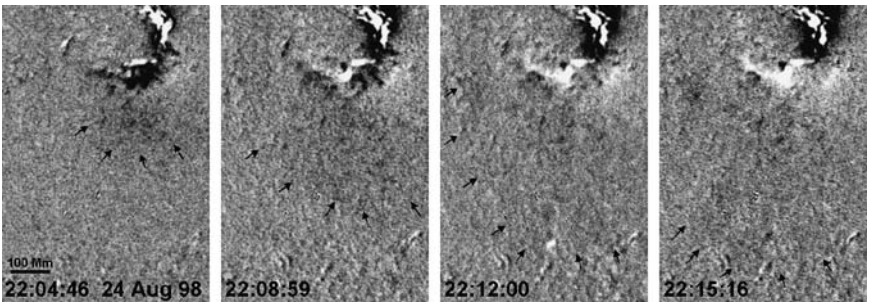

Fig. 9. The He I wave of 1998 August 24 in difference images (*indicated by arrows*). Note its patchy appearance. The flare is seen at the *top* of the images (from [111])

This weakening of absorption in He I is probably due to a reduction of EUV irradiation or heat flux from the corona.

Despite their rather different morphology, He I waves are nevertheless cospatial with both Moreton waves and EIT waves [26, 111]. He I waves also show deceleration, and since they are observed both close to the source AR as well as at larger distances (the temporal cadence is 3 min), they can be regarded as another "missing link" between Moreton and EIT waves (the other one being SXR observations with *GOES*/SXI). Indeed it could be shown for one event that Moreton, EIT and He I wavefronts are consistent with a single decelerating disturbance [111]. Note that despite following similar curves, the He I waves seem to lead the other features by ≈ 30 Mm. An analysis of the He I profiles has revealed that they actually have a two-step shape: a shallow perturbation segment ahead of the corresponding Hα front (*forerunner*), and a main perturbation dip which is cospatial with Hα perturbation.

The waves are also visible in He I velocity data (derived from wing observations), where their behavior is consistent with the downward-upward swing usually observed in Moreton waves [27]. Interestingly, two events were characterized by more than one wave – in one of them, five consecutive waves were observed over a period of less than half an hour [27]. This is puzzling since no such behavior was observed in other wavelength ranges. Either these were very special events or He I is more sensitive to wave signatures than other spectral regimes. The authors suggest that the multiplicity of wavefronts may point to more than one generation mechanism in these events, such as flares *and* CMEs (see Sect. 6).

3.5 Radio: Microwaves and Metric Regime

The Nobeyama radioheliograph [68] observes the Sun at 17 and 34 GHz (microwave regime). Aurass et al. [7] first reported a radio feature moving in the same direction as an EIT wave. Warmuth et al. [118] found three events where actual wavefronts were visible at 17 GHz. These fronts, seen as an increase in

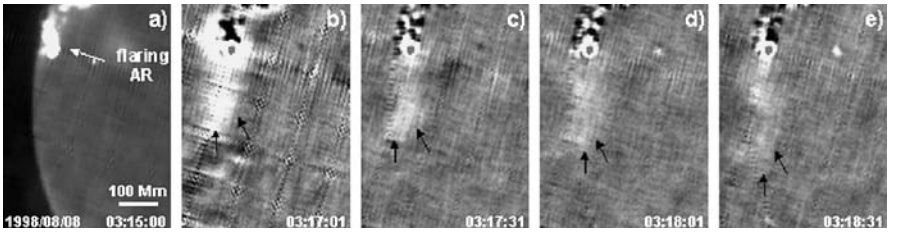

Fig. 10. The coronal wave of 1998 August 8 as shown by 17 GHz difference images (**b**–**e**). Image (**a**) is a pre-event direct radioheliogram showing the flaring active region and the undisturbed chromosphere (from [118])

microwave emission (see Fig. 10), are cospatial with the associated Moreton wavefronts and are also morphologically similar.

White & Thompson [122] have conducted a detailed study of one of these events. They conclude that the bright wavefronts seem to be more consistent with optically thin thermal free-free emission from the corona than with optically thick chromospheric emission. The observed radio brightness temperatures are consistent with the fluxes of the associated EIT wave if the temperature of the emitting gas is not at the peak formation temperature of the Fe XII 195 Å line or if the abundances are closer to photospheric than to coronal values. The radio brightness temperature declines as the wave propagates, which is consistent with the idea of a disturbance decreasing in amplitude.

Recently Vršnak et al. [115] have discovered wave signatures also in the metric regime (at frequencies between 151 and 327 MHz). With the Nançay radioheliograph [45] they observed a broadband radio source that was moving colaterally with an Hα/ EIT wave. The radio emission is interpreted as optically thin gyrosynchrotron emission excited by the passage of the coronal fast-mode shock.

4 Association with Type II Radio Bursts

Coronal waves which have a large amplitude or which are shocked are potential accelerators of particles. Nonthermal electrons generated in this manner can excite Langmuir turbulence which is subsequently converted to electromagnetic radiation (see [64]). Thus, coronal waves could be sources of type II bursts. Indeed there is observational evidence for this scenario. Smith & Harvey [88] reported that $< 50\%$ of Moreton waves were associated with type II bursts, and the comparison of timing and velocities in individual events also suggested a close association between the two phenomena [39, 43].

Recently Warmuth et al. [119] have shown that probably *all* Moreton waves are accompanied by metric type II bursts. The type II bursts in the wave events are $\approx 50\%$ faster and originate lower than an average sample of bursts (for typical type II burst characteristics, see e.g. [16, 60, 84]. This means

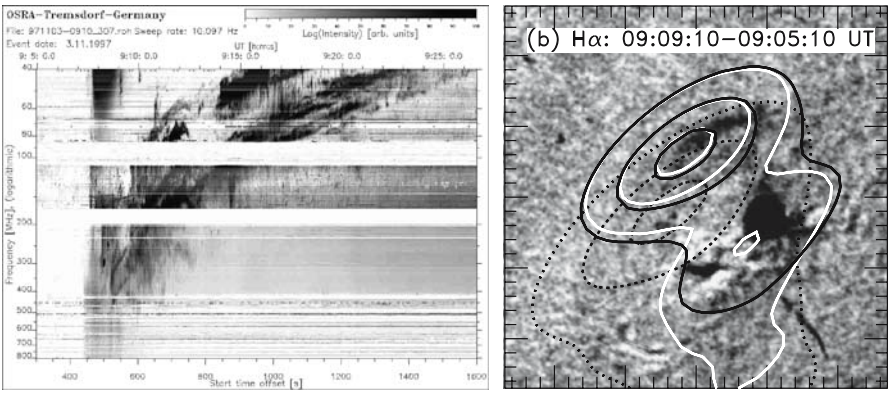

Fig. 11. Left: Metric type II burst associated with a Moreton wave on 1997 November 3 as observed by the Potsdam-Tremsdorf radiospectrograph (see [57]). **Right**: Hα image (Kanzelhöhe Solar Observatory) showing a Moreton wavefront with 30%, 60% and 90% contour levels from a cotemporal Nançay radioheliogram. The type II burst source is cospatial with the Moreton front (from [47])

that they are particularly energetic events. Moreover, close correlations between Moreton and type II kinematics and timing were found, which strongly suggests that Moreton waves and type II bursts are signatures of the same disturbance. This is supported by observations with the Nançay radioheliograph which have shown for two events that the type II burst sources are closely associated with the Moreton wavefronts [47, 78]. One of these examples is shown in Fig. 11.

In four events, [119] measured the band-splitting of the type II emission lanes. Assuming that the band-splitting is due to emission from ahead and behind of the density jump at the coronal shock (e.g. [111]), an Alfvénic Mach number of $M_A \approx 2$ was calculated. Note that this is somewhat higher than the values derived from SXT observations of coronal waves (see Sect. 3.3). It is however consistent with the inferred Mach numbers of the associated Moreton waves [120].

Klassen et al. [49] found that 90% of metric type II bursts are associated with EIT waves. However, the converse is not true: only 21% of EIT waves are accompanied by type II bursts [12]. This suggests that EIT waves are not necessarily associated with coronal shocks, which stands in contrast to the events that do show Moreton wave signatures.

5 The Physical Nature of Coronal Waves

5.1 The MHD Wave/Shock Scenario

We will first discuss the physical nature of the wave events associated with clear chromospheric signatures of Moreton waves because we have a maximum

of observational information for these events. In Sect. 3 we have already shown that the waves observed in the different spectral ranges are closely related: Moreton waves are cospatial with sharp EIT waves, SXT and SXI waves, He I waves and waves seen in 17 GHz as well as in metric radioheliograms. Deceleration seems to be a general property of the physical disturbance causing these signatures, which means that also the more remote diffuse EIT waves can be generated by the same perturbation. This is supported by SXI and He I data which bridge the gap between Moreton and EIT wave observations.

The morphology of the signatures (e.g. the fact that they are consisting of enhancements of pre-existing structures) suggests that the common agent is a wave and not, for example, a bulk mass motion like a flare spray. This is strongly supported by the nearly perfect circular curvature of the leading edges of Moreton wavefronts close to their source point [118]. The observed down-up swing of the chromosphere observed in Hα and He I further implies that the impact of a coronal wave leads to the creation of Moreton and He I wave signatures.

Coronal waves are observed over a considerable temperature range (EUV to SXR) and must therefore be compressive, which is independently shown by the microwave data which are sensitive to density enhancements rather than to temperature changes. The waves travel along the solar surface, and since the magnetic field is oriented radially in the quiet Sun, they propagate perpendicularly to the magnetic field. In addition, they are faster than the coronal sound speed (e.g. [62]). These facts suggest that the waves are fast-mode MHD waves (slow-mode waves cannot propagate perpendicular to the magnetic field), and since $\theta_B \approx 90^\circ$ we can treat them as magnetosonic waves.

It should be stressed that the disturbances tend to decelerate to comparable speeds at larger distances, e.g. the mean EIT wave speed given by [118] is $\langle \bar{v}_{\rm EIT} \rangle = 311 \pm 84$ km s^{-1} while a different sample in [121] yielded $\langle \bar{v}_{\rm EIT} \rangle = 320 \pm 120$ km s^{-1}. This implies that in the late phase of the events, the velocities do not reflect the properties connected to an individual event (e.g. the speed of ejected matter in an eruptive scenario), but rather the conditions of the ambient medium (i.e. the magnetosonic speed). This supports the notion that the disturbances are MHD waves.

The magnetosonic speed in the quiet low corona, as given by several authors, is in the range of $\approx$200–600 km s^{-1} [70, 116, 125]. This is consistent with typical EIT wave velocities, but the initial speeds of coronal waves are significantly higher, on the order of 1 000 km s^{-1}. This means that at least initially the waves must be shocked, with magnetosonic Mach numbers of up to $M_{ms} \approx$ 2–3, as shown for two events in Fig. 12 [120]. Note that also large-amplitude simple waves [59, 106] can move faster than the characteristic speed of the medium. However, a coronal wave can maintain a Mach number of greater than unity over a considerable distance range which means that also its leading edge has to move faster than the characteristic speed. This is only possible for a shock.

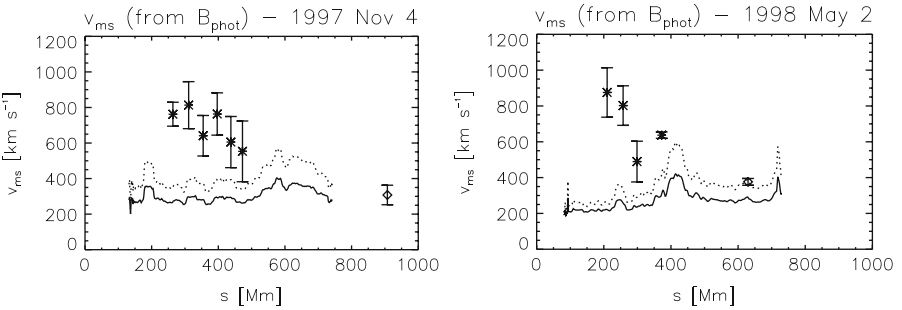

Fig. 12. Comparison of the magnetosonic speed v_{ms} as a function of distance s from the source AR (derived from the measured photospheric magnetic field strength) with measured wave speeds for the events of 1997 November 4 and 1998 May 2. The *solid* and *dotted lines* are the $v_{ms}(s)$ derived for a coronal magnetic field strength of 1/3 and 1/2 times the photospheric value, respectively. *Asterisks* denote Hα Moreton wave speeds, *diamonds* represent EIT wave speeds (after [120])

The shock scenario is supported by the basic characteristics of the waves (deceleration, perturbation broadening and weakening), which are consistent with a shock formed from a large-amplitude simple MHD wave. The simple MHD wave needs time to steepen into a shock which explains both the fact that coronal waves are never observed in the immediate vicinity of their source location. Eventually the shock decays to a linear (i.e. small-amplitude) fast-mode wave (cf. Sect. 2).

An independent confirmation of the shock scenario comes from *Yohkoh*/SXT observations of coronal waves. Using filter ratio methods, Narukage et al. [70] and Hudson et al. [41] have shown that the intensities of coronal waves are consistent with fast-mode shocks. Furthermore, it seems that all Moreton waves are accompanied by metric type II burst, another evidence for a coronal shock. Correlations between the kinematics and timing of Moreton waves and radio bursts, as well as direct comparisons of the locations of wavefronts and burst sources, suggests that coronal waves and type II bursts can be attributed to the same coronal shock.

Figure 13 shows how the different observational signatures are created in this scenario. The curves below the main graph show idealized intensity profiles of the waves seen in Hα line center and He I (upper plot), the Doppler velocity profile (middle) and the profiles in the wings of Hα (lowermost plot). The variable r denotes the distance from the origin of the wave. Since the coronal magnetosonic speed increases with height in the low corona [62], the shock front is slightly inclined to the magnetic field lines. This is actually observed in limb events [41] and reproduced by numerical simulations [125]. The tilting is also consistent with the "premature" filament activation reported by Eto et al. [23]. The filament (F in Fig. 13) is located higher up in the corona, and is thus activated before the lower parts of the shock have actually

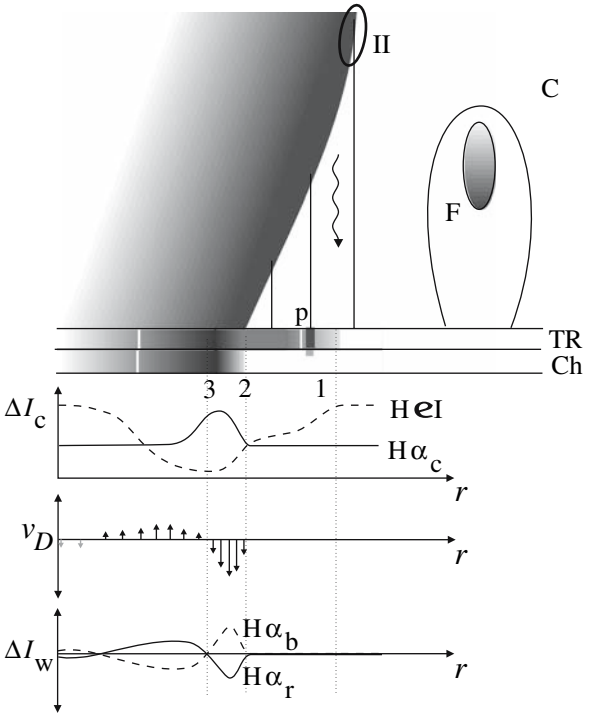

Fig. 13. Schematic presentation of the fast-mode MHD shock passage through the corona (C) and its signatures in the transition region (TR) and chromosphere (Ch). For details see main text (from [119])

reached it. On the disk, the visible EIT wavefront coincides with the lower part of the shock, since the largest fraction of the observed emission is generated there, and the comparatively tenuous upper parts of the wavefront are only observable in limb events.

The downstream coronal plasma is compressed and heated by the shock, creating the wavefronts seen in EUV and SXR. The chromospheric plasma is pushed down by the pressure increase at the coronal base (at $r = 2$), which is observed as the Moreton wave in both Hα line center and wings, Should compressive heating also be taking place in the chromosphere, this would show up as optically thick microwave emission. Alternatively, the compression of the coronal plasma may generate wavefronts in the microwave regime via optically thin free-free emission [122]. After being pushed down the chromosphere relaxes, creating the trailing wavefronts seen in the wings of Hα ($r = 3$).

The pressure jump at and behind the shock causes an increase in density and temperature in the transition region as well. The enhancement of collisional processes could create the main perturbation segment in He I ($r = 2$ in Fig. 13). The He I forerunner ($r = 1$) indicates that processes are influencing

the He I absorption already before the shock arrival. The observation that the He I absorption is particularly increased in discrete patches associated with magnetic field concentrations (p) suggests that some agent is propagating down from the higher parts of the shock along the field lines. This could be due to thermal conduction from the shocked coronal plasma or due to electrons accelerated at the quasi-perpendicular segment of the shock (wavy arrow in Fig. 13; see [111]), where also the type II burst source is located (II). An alternative explanation would be increased EUV irradiation from the coronal plasma.

The presented model integrates all observational signatures of coronal waves. However, thus far we have only focused on the relatively few events that are associated with both prominent Moreton waves and metric type II bursts. After all, EIT waves have a frequency of occurrence that is about one order of magnitude larger than that of Moreton waves, and only 21% of EIT waves are associated with type II bursts [12].

It may be that in most coronal waves the perturbation is weaker than in the events we have considered. If the wave does not steepen to large amplitudes, or to a shock, no electrons will be accelerated, and consequently no type II burst will be observed. At the same time, a comparatively weak coronal wave will have difficulty perturbing the more inert chromosphere, and no or only weak Moreton wave signatures will be observed. Filaments and coronal loops, on the other hand, appear to be more susceptible towards the impact of coronal waves since they are often excited to oscillate without direct observations of coronal waves [42, 88].

5.2 Alternative Scenarios: Magnetic Reconfiguration

There are of course alternatives to the MHD wave/shock scenario presented above, which are particularly attractive for the weak events (i.e. events without Hα signatures and type II bursts) discussed at the end of the previous section. Inconsistencies between the wave interpretation and EIT observations have first been pointed out by Delannée & Aulanier [20], who noted that in some EIT wave events parts of bright fronts can remain stationary for a prolonged time. Moreover they noted that the bright fronts are followed by an expanding area of coronal dimming. These findings led Delannée & Aulanier [20] to argue that EIT waves are not MHD waves, but rather the consequence of the reconfiguration of magnetic field lines during a CME lift-off.

In this scenario, the stationary bright fronts are due to the compression of the plasma near the footpoints of opening magnetic field lines located close to the separatrix. Dependent on the magnetic topology, such a front might also be propagating as the field opens up further and further from the CME launch site. Such a propagation can be halted when the bright front encounters regions of more or less vertical fields, such as coronal holes or the footpoints of large loops. This was also observed in several cases [21]. Another possibility is that the moving fronts are produced by the interaction of

sheared expanding magnetic field lines with surrounding field lines that are nearly potential [21]. This interaction could produce local electric currents, leading to heating that could account for the emission increase in the bright fronts.

Another implication of this scenario is that due to the expansion of the magnetic field lines behind the bright fronts the local plasma density is decreased, which can account for the coronal dimming. Lastly, the fact that CME eruptions often involve large-scale structures such as transequatorial interconnecting loops (TILs) accounts for the observation that many EIT waves are propagating anisotropically, in contrast to such textbook events like the 1997 May 12 event reported by Thompson et al. [92].

In order to obtain more quantitative results (i.e. with respect to propagation velocities), Chen et al. [14] made a numerical simulation of an erupting flux rope and looked for CME-induced wave phenomena. They found that the erupting flux rope drives a piston shock in front of it (see Fig. 14). While the top of this CME-driven coronal shock generates the type II radio burst, its flanks extend down to the solar surface where they can produce Moreton waves (at low altitudes, the shock may degenerate to a finite-amplitude MHD wave). Simultaneously, behind the flanks of the shock a plasma density enhancement is propagating at a lower speed. This feature is due to successive stretching or opening of closed field lines covering the erupting flux rope, and based on its velocity it is interpreted as the EIT wave, which is thus not actually a wave in the physical sense. Corresponding to the plasma enhancement in the EIT front, plasma gets evacuated in the inner region behind the front. This can explain the dimming commonly observed behind EIT waves.

Chen et al. [15] have extended this model by considering a case where two smaller ARs are placed on either side of the erupting flux rope. They found that the density enhancement interpreted as the EIT front stops at the boundary of active regions and coronal holes, which nicely reproduces the behavior of stationary EIT fronts.

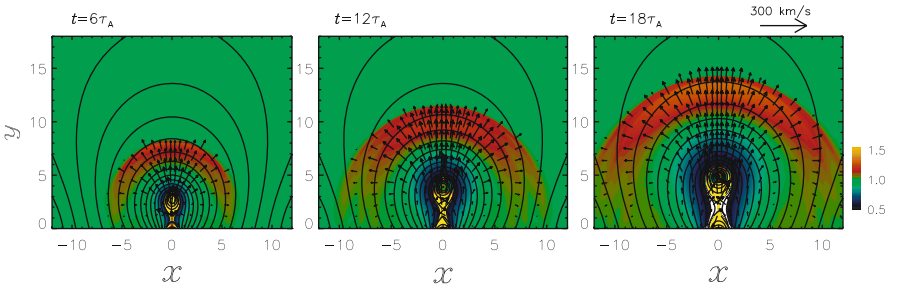

Fig. 14. Evolution of the density (*gray scale*), magnetic field (*solid lines*), and velocity (*arrows*) in the scenario by Chen et al. A piston-driven shock straddles the erupting flux rope, with the flanks sweeping the solar surface and an expanding dimming region lagging far behind (from [15])

The Chen model could be considered as a hybrid between the wave/shock scenario and Delannée's proposal. It explains the velocity discrepancy between Moreton and EIT waves by invoking two physically distinct disturbances, and succeeds in reproducing many observational findings, i.e. that the type II speed is correlated with the Moreton speed, but not with the EIT wave speed. However, it fails in a crucial point: in the well-studied events that have prominent Moreton waves there is no observational evidence for two distinct disturbances. On the contrary, observations linking Hα and EIT observations have clearly shown that a single decelerating disturbance is responsible for both the fast Moreton and the slow EIT wave. Chen et al. [15] argue that in those cases the EIT fronts that are observed are actually the coronal Moreton wave, whereas the predicted slower perturbation is below the observational threshold. In fact, this would fully confirm the wave/shock scenario presented in Sect. 5.1, with the addition of a slow trailing disturbance that seems to be energetically insignificant in most events. In events without Moreton signatures this slow disturbance would nicely reproduce some characteristics of EIT waves (e.g. partly stationary fronts), but why would the perturbation clearly show up in EIT only in those events and not also in the presumably more energetic Moreton-associated events?

Leaving these questions aside, the observation of stationary bright fronts and dimming is actually not in itself sufficient to rule out the wave/shock scenario. In principle, also waves and shocks can trigger localized energy release when they cross pre-existing coronal structures, leading to localized heating and a stationary emission enhancement (cf. [73]). This was possibly the case for a coronal wave observed in the metric regime by Vršnak et al. [115]. When the wave passed enhanced coronal structures, the radio emission became prolonged, indicating that a local energy release was triggered by the disturbance.

The wave/shock scenario does not claim to explain dimming, but it also does not preclude the launch of a CME (which is indeed observed in many events) which would lead to coronal dimming. The dimming could therefore be connected to the CME and not to the wave itself. The observation that the dimming area generally follows the wave may imply that the CME plays an important role in launching or driving the wave. However, the association between dimming and wavefronts is not always very close. For example, in the event studied by Thompson et al. [94], the dimming area was located only behind the eastern half of the bright front. This implies that wavefronts and dimming need not necessarily be as tightly related as the magnetic reconfiguration scenario predicts, where the dimming should always follow the bright fronts very closely.

It may well be that many EIT waves are not MHD waves but rather signatures of a restructuring of coronal magnetic fields, e.g. in the framework of an eruption (e.g. [24, 37]). In particular, this seems to be a fitting scenario for EIT waves that have a very irregular shape or which are very slow or show some kind of erratic propagation. The other extreme

of the event spectrum – coronal waves that are associated with prominent Hα signatures and metric type II bursts – shows quite different characteristics that are better reproduced by the wave/shock scenario (Sect. 5.1). In particular, it should be pointed out that all wave signatures in these events are created by a common disturbance that is closely related with the associated metric type II burst. Since type II bursts can only be generated by an MHD shock (and not by magnetic reconfiguration), this implies that also the propagating fronts are created by an MHD shock or wave.

6 Causes of Coronal Waves

While a lot of progress has recently been made regarding the physical nature of coronal waves, their actual causes remain elusive. The same is true for metric type II bursts. It is quite clear that a sudden disturbance has to be introduced into the corona in order to launch large-scale waves or shocks, but there are several candidates for the initial perturbation. Usually, a "flare-driven" and a "CME-driven" scenario are discussed, but the situation is actually more complex than this.

Historically, Moreton waves were first linked to *solar flares* (hence the term *flare waves*) since they are always associated with them. It was noted that the flares in Moreton events were characterized by an "explosive phase" characterized by a sudden increase in brightness and a rapid expansion of the flare borders during the impulsive phase (e.g. [3]). This led to the classical pressure-pulse model where the rapidly expanding flaring volume (effectively acting as a spherical piston; cf. Sect. 2) launches a freely propagating blast wave (see [107]).

Alternatively, *small-scale ejecta* have been proposed as possible causes of coronal waves and shocks. This is based on their speeds which can be comparable to typical Moreton wave speeds (e.g. [108]), as well as on the fact that they are often associated with coronal waves. Flare sprays, observed in Hα, are present in many Moreton wave events [91, 130]. More recently, additional types of flare ejecta have been observed with *Yohkoh*/SXT, such as X-ray jets, plasmoids and erupting loops (e.g. [74, 87]). There is evidence for the generation of metric type II bursts by rapidly expanding X-ray structures [28, 32, 50, 51]. Since these bursts are closely associated with coronal waves, the waves could possibly be launched in the same manner. Physically, such an ejection would act as a temporary piston, generating an initially driven shock. After the ejection stops or decelerates, the disturbance continues as a freely propagating blast wave. Thus in the later stages, there is no difference between the pressure-pulse and the ejection scenario.

The discovery of *coronal mass ejections* in the 1970s led to the "piston-driven" theory of type II bursts (e.g. [17, 33, 89], and references therein). In this scenario a CME acts as a piston creating a driven shock, which can result in a type II burst and/or in a coronal wave.

With regard to the cause of type II bursts, no consensus has yet been reached. There is evidence that both flares *and* CMEs can create shocks (e.g. [16, 86]), but it seems that the flare-generated disturbances usually cannot penetrate to IP space, since most of those bursts cease at $\simeq$ 20 MHz [29]. This is probably due to a local maximum of the Alfvén speed in the higher corona [63]). Therefore, most hectometric/kilometric type II bursts seem to be generated by CME-driven shocks (e.g. [13, 34]).

Let us consider the more complicated situation in the corona in more detail. An excellent timing association of metric type II bursts with the impulsive phase was found (e.g. [48, 90, 105, 109]). Unfortunately this is actually an ambiguous result since the CME acceleration phase is often synchronized with the impulsive energy release of the associated flare (e.g. [113, 127, 128]). Another approach is to look for correlations between various wave/shock characteristics and the flare energy release or CME characteristics. A range of relatively well defined correlations was found for flares (e.g. [76, 109, 110]). Analoguous correlations with CME parameters are either absent or have a low statistical significance [82] unless long-wavelength bursts are also considered. Based on these results, one might suppose that coronal type II bursts are mainly launched by flares. However, since there are type II bursts that extend from the metric regime up to hectometric-kilometric regime (Gopalswamy, this volume), a certain fraction of coronal shocks is probably created by CMEs.

If CMEs are able to create type II bursts in the low corona, they may also be responsible for (some) coronal waves. The most straightforward possibility is that they drive coronal shocks which show up as wavefronts near the solar surface. Another possibility is that they generate fronts that are not due to MHD waves but rather the result of opening magnetic field lines (cf. the discussion in Sect. 5.2). Irregular EIT waves without associated Moreton waves and type II bursts are possibly generated in the latter manner, while the "strong" wave events – with sharp circular Moreton wavefronts, possibly sharp EIT and SXR fronts and type II bursts – seem to be more consistent with a real MHD wave/shock. A third possibility is that the launch of a CME generates an initial pressure pulse which quickly becomes a freely propagating blast wave, much in the same manner as in the flare and small-scale ejection scenarios (e.g. [27]).

How can we distinguish between the different possibilities? An obvious starting point would be to see which associated phenomena are present in coronal wave events. Unfortunately, in the events with prominent Moreton waves flares, small-scale ejecta and CMEs all seem to be present. For EIT waves in general, several authors have used statistical arguments to show that CMEs are a more important ingredient for the production of EIT waves than flares are [12, 20]. At the other end of the event spectrum there are coronal waves which are associated with neither of the potential causes (e.g. [121]).

Researchers are just now beginning to investigate the important issue of the waves' origin, but let us consider some preliminary results anyway. One would expect that a wave caused by a CME, which is a large-scale

phenomenon, does not originate from a "point source" such as a flare but from a comparatively extended area. There are reports of flare-associated CMEs which originate from structures with comparatively small sizes, such as the events reported by Neupert et al. ([71]; see also [5]). Still, the preexisting AR loops which were identified as the source of the later CME loops had dimensions of 100–250 Mm. The Moreton waves of Warmuth et al. [118] were first observed $\approx$100 Mm from the source point, where they had a nearly perfect circular curvature and were very sharp. It is difficult to imagine how an extended source such as a CME, even such an initially "compact" CME, could create such signatures. On the other hand, the source point of the waves generally seems to be displaced from the flare center, which is inconsistent with a simple point-like explosion. One might speculate that strong magnetic fields in the active region could provide a guiding of the wave until the outskirts of the AR are reached, where the wave starts to spread out (Huygens' principle). Alternatively, fast-small scale ejecta such as flare sprays might account for the offset.

Regarding the possibility of the CME directly driving a shock as a piston, it should be pointed out that CMEs are accelerating in the low corona (e.g. [127]), whereas coronal waves are decelerating. This rules out the possibility that coronal waves are created by a shock driven by the leading edge of a CME (unless the shock quickly becomes freely propagating in the low corona). However, the flanks of a CME remain fixed during much of the later phase of the eruption, which implies that they have to decelerate somewhere. This means that they could in principle drive a shock that is consistent with the observed wavefronts. This is an important issue for further work, since the kinematical behavior of CME flanks is presently not well understood.

These first results are not sufficient to positively identify the waves' generation mechanism. It is interesting to note, though, that coronal waves that are associated with Moreton waves and metric type II bursts are always accompanied by impulsive flares and/or high-velocity small-scale ejecta. Whether these phenomena constitute a necessary ingredient for the waves' generation remains to be determined. In these events the launch of the waves is closely associated with the impulsive phase of the flares [41, 47, 121], just as it was found for metric type II bursts. Again, the possibly close synchronization of the CME acceleration phase with the impulsive phase of the flare does not allow an unambiguous conclusion.

Many coronal disturbances are not associated with flares or type II bursts, and consequently the situation is much less ambiguous for those events. They may be launched by CMEs or they may be consequences of a restructuring of the coronal magnetic fields (cf. Sect. 5.2). It is also possible that more than one process is working in a single event (cf. [27]).

To make further progress regarding the cause of coronal waves, multiwavelength high-cadence observations of the launch of coronal waves, as well as of the associated flares, small-scale ejecta and CMEs will be required. In addition to radio observations and ground- as well as space-based coronagraphs the

space missions *TRACE* [35] and *RHESSI* [55] are particularly important for this task. *TRACE* provides high-cadence and high-resolution observations of coronal processes such as ejections, and might be able to resolve the initiation stage of a coronal wave. The hard X-ray observations of *RHESSI*, on the other hand, allow a detailed analysis of flare energetics.

7 Relevance of Coronal Waves to Other Areas of Solar Physics

Apart from being interesting in themselves and providing information on the flare/CME process, coronal waves can be used to illuminate other aspects of solar physics. In the following, three different "applications" are discussed.

7.1 Particle Acceleration

Coronal waves can have a large amplitude, which means that they are either shocks or large-amplitude simple waves. Both kinds of disturbances are able to accelerate particles, thus they may represent an additional source of *solar energetic particles* (SEPs), which are commonly assumed to be generated at CME-driven interplanetary shocks (for a review, see [81]). Since coronal waves are globally propagating, they can provide an explanation for SEP events that are associated with flares that have a large distance from the Earth-connected magnetic field lines in the western hemisphere of the Sun.

Kocharov et al. [52] first reported the observation of a Moreton wave and an associated SEP event. Based on timing arguments, they concluded that electrons as well as protons are promptly accelerated at the Moreton-associated shock. Torsti et al. [95, 96] claimed that the calculated proton release times are close to the times when EIT waves reach the western limb. A large sample of impulsive electron events was studied by Krucker et al. [53]. For 3/4 of the events that were not related to the flare-associated type III bursts, EIT waves were observed. Krucker et al. conclude (using timing and spatial arguments) that at least some of the impulsive electron events are more likely related to the propagating wave than to the flare itself.

Recently Vainio & Khan [103] have considered particle acceleration at a refracting coronal shock, which means a scenario where the shock front becomes tilted towards the solar surface due to the increase of v_A with height in the low corona (cf. Fig. 13). They noted that in this geometry it is possible that the observer at 1 AU is magnetically connected to the downstream region of the shock (see Fig. 15). Diffusive shock acceleration then results in a power-law spectrum of the accelerated ions – a result which is not naturally obtained when the observer is connected to the upstream region of the shock (as it is the case in the classical CME-driven bow shock scenario). Acceleration in such refracting shocks may also provide a preacceleration mechanism for further acceleration CME-driven shocks in large gradual SEP events.

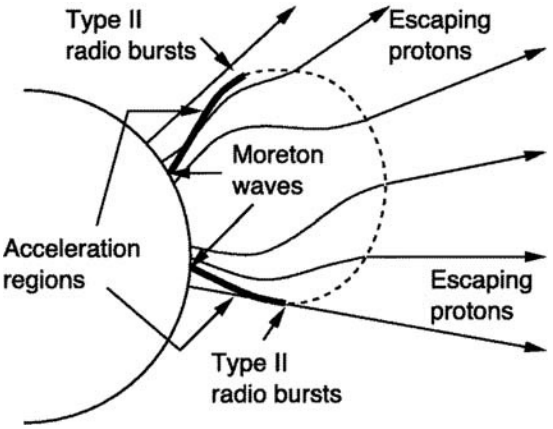

Fig. 15. Global shock geometry of a refracting coronal shock (from [103])

7.2 Coronal Loop Oscillations

The coronal magnetic field is highly elastic, and it is thus expected that it can be excited to oscillate (for theoretical considerations, see e.g. [83]). *TRACE* has indeed observed oscillating coronal loops [2, 69, 85]. These loops oscillate with periods of a few minutes and are damped after a few cycles. This behavior can be explained as a *kink mode* oscillation in which the loop is bodily displaced while the footpoints remain fixed.

The oscillations appear to be excited by nearby flares and filament eruptions. Thus it is well possible that coronal waves launched by the flare/eruption initiate the oscillations. Hudson & Warmuth [42] have supported this scenario through a statistical analysis of 30 oscillation events. In particular, a comparatively high association with metric type II bursts (12 out of 30 events) was found, and the timing of flare/oscillation/type II burst is consistent with the notion that the oscillations are excited by a blast wave associated with the type II burst. This scenario is further supported by the analogy with "winking filaments" and at least one case where a coronal wave is directly observed to excite a loop to oscillate [124].

7.3 Coronal Seismology

Coronal seismology (cf. [83]) is a relatively new diagnostic tool that uses the observed properties of MHD waves and oscillations in order to determine physical parameters of the corona that are otherwise not observable, for example the coronal magnetic field strength. Longitudinal compressive waves in polar plumes [18] and coronal loops [10] and transverse coronal loop oscillations (e.g. [69]) have been used in this manner.

Global properties of the quiet corona, on the other hand, can be derived by studying the propagation of global coronal waves. Mann et al. [62, 63]

have equated the mean EIT wave speed with the magnetosonic speed v_{ms} in the quiet corona. A more detailed study has recently been conducted by Warmuth & Mann [120], where values around 3 G were obtained for the magnetic field strength in the quiet low corona. Ballai & Erdélyi [8] have used the velocity attenuation of EIT waves to derive viscosity coefficients over an order of magnitude higher than the classical value. Note that this approach is only valid if the waves are not shocked and do not have a large amplitude.

8 Conclusions

There has been evidence for the presence of globally propagating, large-scale waves and shocks in the solar corona since more than 50 years. Prompted by spaceborne observations of the corona as well as by high-cadence ground based observations of the chromosphere the recent years have seen a dramatic expansion of our knowledge of these phenomena. Particularly, a large number of global wavelike disturbances has been observed by the *SOHO*/EIT instrument ("EIT waves"). Starting from Hα observations of chromospheric Moreton waves, corresponding wave signatures have been found in the near-IR Helium I line, in the EUV and SXR regime, as well as in radioheliograms. The various signatures all follow closely associated kinematical curves and display deceleration. This implies a common underlying disturbance and resolves the apparent "velocity discrepancy" between Moreton and EIT waves.

The typical characteristics of the common disturbance are deceleration, combined with a broadening of the perturbation profile and a decrease of its amplitude. This is typical for a freely propagating fast-mode MHD shock created by a large-amplitude perturbation (a nonlinear "simple wave"; see [59, 106]). As the shock propagates, its amplitude decreases, which also leads to a deceleration of the disturbance. The presence of a shock is further underlined by the observation of closely associated metric type II radio bursts in all Moreton events. Finally, the shock decays to an ordinary (small-amplitude) fast-mode wave which is supported by the observation that coronal waves decelerate to comparable velocities.

In principle, this scenario is similar to the classical blast-wave model by Uchida [99]. For the "strong events" – those with high initial velocities, clear chromospheric signatures, sharp wavefronts and associated type II bursts – this model fits the observational constraints better than alternative proposals. The wave/shock scenario is particularly supported by the close association found between the coronal waves and metric type II bursts, which can only be generated by an MHD shock. However, it seems that these events form a special class since the majority of coronal waves does not show these characteristics. It may be that in most cases the wave does not steepen to a large amplitude or to a shock, which means that it will become difficult for the wave to perturb the more inert chromosphere. Also, no electrons will be accelerated, and consequently no type II burst will be generated. Alternatively,

such "weak events" may not be MHD waves at all in a physical sense, but rather signatures of the restructuring of coronal magnetic fields [15, 21]. This may be a fitting scenario for waves that have an irregular shape, a low speed, or which show some kind of erratic propagation.

At this point a few words have to be said regarding the terminology of coronal waves and shocks. At the moment, there exists a multitude of partly overlapping terms that describe different aspects of these disturbances, and even different physical processes. What is worse is that the usage of terms is somewhat arbitrary and even contradictory at times. A more exact usage of terms is therefore necessary. "Coronal wave" should exclusively be used for moving features that are most likely waves (including large-amplitude simple waves and shocks), such as the "strong events" that are associated with Moreton waves and metric type II bursts. These events actually form a well-defined class: they are all characterized by a wavefront with a relatively smooth shape close to the source AR, a decelerating motion with a mean deceleration of a few 100 $\mathrm{m\,s^{-2}}$ and speeds around 300 $\mathrm{km\,s^{-1}}$ at large distances from the AR.

"Coronal wave" should be considered as the general term referring to the physical disturbance. When there is a need to differentiate these phenomena from other waves in the corona, they can be called "large-scale coronal waves". Terms like "Moreton wave" or "EIT wave" can be used when discussing observations from the respective instruments or spectral ranges. For the multitude of other moving coronal features whose physical nature has yet to be determined, the term "wave" should be avoided altogether. Instead, more general terms such as "coronal transient" or "moving coronal disturbance" should be used. It is true that even the "coronal waves" defined according to the criteria given above are not unambiguously identified as true waves yet. However, as long as there is no convincing evidence to the contrary, the term coronal waves should be retained (though used more discriminately) as it is convenient, has become widely used and reflects the current view of the majority of the solar physics community. A detailed discussion of the issue of terminology can be found in Vršnak [114].

The causes of coronal waves are still unclear. In principle, flares, small-scale ejecta and CMEs are viable mechanisms for the generation of large-amplitude disturbances, while large-scale eruption such as CMEs seem to be the necessary ingredient within the framework of a magnetic reconfiguration scenario. Careful multiwavelength observations of individual events as well as statistical studies will be needed to resolve this issue.

The mere presence of coronal waves signifies that some very impulsive and violent processes must be happening in the early impulsive phase of flares and/or during a CME launch. Coronal waves are thus not only interesting in themselves, but also relevant to other issues in solar physics, including acceleration of solar energetic particles and excitation of loop oscillations. They can even be used to probe the corona for parameters that are otherwise not observable ("coronal seismology"). In order to get a deeper insight into

these phenomena, we will need improved observational capabilities which will hopefully be provided by the upcoming missions STEREO and Hinode.

Acknowledgements

I wish to thank the organizers of the CESRA workshop for a particularly stimulating meeting. I also thank G. Mann, H. Aurass and B. Vršnak for fruitful discussions. This work was supported by DLR under grant No. 50 QL 0001.

References

1. Andretta, V., & Jones, H. P.: Astrophys. J. **489**, 375 (1997) 117
2. Aschwanden, M. J., De Pontieu, B., Schrijver, C. J., & Title, A. M.: Solar Phys. **206**, 99 (2002) 131
3. Athay, R. G., & Moreton, G. E.: Astron. J. **133**, 935 (1961) 108, 127
4. Aurass, H.: in *Coronal Physics from Radio and Space Observations*, ed. G. Trottet (Springer, Berlin 1997), Lect. Notes Phys. **483**, 135 107
5. Aurass, H., Vourlidas, A., Andrews, M. D., Thompson, B. J., Howard, R. H., & Mann, G.: Astrophys. J. **511**, 451 (1999) 129
6. Aurass, H., Vršnak, B., & Mann, G.: Astron. Astrophys. **384**, 273 (2002a) 108, 109
7. Aurass, H., Shibasaki, K., & Reiner, M.: Astrophys. J. **567**, 610 (2002b) 118
8. Ballai, I., & Erdélyi, R.: in *Proceedings of SOHO 13 – Waves, Oscillations and Small-Scale Transient Events in the Solar Atmosphere*, ed. H. Lacoste, ESA SP-547, 433 (2004) 132
9. Becker, U.: Z. Astrophys. **44**, 243 (1958) 107
10. Berghmans, D., & Clette, F.: Solar Phys. **186**, 207 (1999) 131
11. Biesecker, D. A., & Thompson, B. J.: J. Atmos. and Sol.-Terr. Phys. **62**, 1449 (2000) 107
12. Biesecker, D. A., Myers, D. C., Thompson, B. J., et al.: Astrophys. J. **569**, 1009 (2002) 114, 120, 124, 128
13. Cane, H. V., Sheeley, N. R., Jr., & Howard, R. A.: J. Geophys. Res. **92**, 9869 (1987) 107, 128
14. Chen, P. F., Wu, S. T., Shibata, K., & Fang, C.: Astrophys. J. **572**, L99 (2002) 125
15. Chen, P. F., Fang, C., & Shibata, K.: Astrophys. J. **622**, 1202 (2005) 125, 126, 133
16. Classen, H. T., & Aurass, H.: Astron. Astrophys. **384**, 1098 (2002) 119, 128
17. Cliver, E. W., Webb, D. F., & Howard, R. A.: Solar Phys. **187**, 89 (1999) 108, 127
18. DeForest, C. E., & Gurman, J. B.: Astrophys. J. **501**, L217 (1998) 131
19. Delaboudinière, J.-P., Artzner, G. E., Brunaud, J., et al.: Solar Phys. **162**, 291 (1995) 114
20. Delannée, C., & Aulanier, G.: Solar Phys. **190**, 107 (1999) 124, 128
21. Delannée, C.: Astrophys. J. **545**, 512 (2000) 124, 125, 133
22. Dodson, H. W.: Astrophys. J. **110**, 382 (1949) 107
23. Eto, S., Isobe, H., Narukage, N., et al.: PASJ **54**, 481 (2002) 115, 122
24. Foley, C. R., Harra, L. K., Matthews, S. A., et al.: Astron. Astrophys. **399**, 749 (2003) 126

25. Gilbert, H. R., Thompson, B. J., Holzer, T. E., Burkepile, J. T.: AGU Fall Meeting 2001, abstract SH12B-0746 (2001) 117
26. Gilbert, H. R., Thompson, B. J., Holzer, T. E., Burkepile, J. T.: Astrophys. J. **607**, 540 (2004) 117, 118
27. Gilbert, H. R., & Holzer, T. E.: Astrophys. J. **610**, 572 (2004) 118, 128, 129
28. Gopalswamy, N., Kundu, M. R., Manoharan, P. K., et al.: Astrophys. J. **486**, 1036 (1997) 127
29. Gopalswamy, N., Kaiser, M. L., Lepping, R. P., et al.: J. Geophys. Res. **10**, 307 (1998) 128
30. Gopalswamy, N., & Thompson, B. J.: J. Atmos. and Sol.-Terr. Phys. **62**, 1457 (2000) 116
31. Gopalswamy, N., Kaiser, M. L., Sato, J., & Pick, M.: in *High Energy Solar Physics – Anticipating HESSI*, eds. R. Ramaty & N. Mandzhavidze (Astronomical Society of the Pacifc, San Francisco 2000), ASP Conf. Ser. **206**, 351 114
32. Gopalswamy, N., St. Cyr, O. C., Kaiser, M. L., & Yashiro, S.: Solar Phys. **203**, 149 (2001) 127
33. Gosling, J. T., Hildner, E., MacQueen, R. M., et al.: Solar Phys. **48**, 389 (1976) 127
34. Gosling, J. T.: J. Geophys. Res. **98**, 18937 (1993) 128
35. Handy, B. N., Acton, L. W., Kankelborg, C. C., et al.: Solar Phys. **187**, 229 (1999) 114, 130
36. Harra, L. K., & Sterling, A. C.: Astrophys. J. **561**, L215 (2001) 116
37. Harra, L. K., & Sterling, A. C.: Astrophys. J. **587**, 429 (2003) 126
38. Harrison, R. A., Bryans, P., Simnett, G. M., & Lyons, M.: Astron. Astrophys. **400**, 1071 (2003) 116
39. Harvey, K. L., Martin, S. F., & Riddle, A. C.: Solar Phys. **36**, 151 (1974) 108, 119
40. Hill, S. M., Pizzo, V. J., Balch, C. C., et al.: Solar Phys. **226**, 255 (2005) 117
41. Hudson, H. S., Khan, J. I., Lemen, J. R., et al.: Solar Phys. **212**, 121 (2003) 116, 122, 129
42. Hudson, H. S., & Warmuth, A.: Astrophys. J. **614**, L85 (2004) 124, 131
43. Kai, K.: Solar Phys. **11**, 310 (1970) 119
44. Kantrowitz, A. & Petschek, H. E.: in *Plasma in Theory and Application*, ed. W. B. Kunkel (McGraw Hill, Oxford 1966), 148 111
45. Kerdraon, A., & Delouis, J.-M.: in *Coronal Physics from Radio and Space Observations*, ed. G. Trottet (Springer, Berlin 1997), Lect. Notes Phys. **483**, 192 119
46. Khan, J. I., & Hudson, H. S.: Geophys. Res. Lett. **27**, 1083 (2000) 116
47. Khan, J. I., & Aurass, H.: Astron. Astrophys. **383**, 1018 (2002) 114, 117, 120, 129
48. Klassen, A., Aurass, H., Klein, K.-L., Hofmann, A., & Mann, G.: Astron. Astrophys. **343**, 287 (1999) 128
49. Klassen, A., Aurass, H., Mann, G., & Thompson, B. J.: Astron. Astrophys. Suppl. **141**, 357 (2000) 114, 120
50. Klassen, A., Pohjolainen, S., & Klein, K.-L.: Solar Phys. **218**, 197 (2003) 127
51. Klein, K.-L., Khan, J. I., Vilmer, N., et al.: Astron. Astrophys. **346**, L53 (1999) 127
52. Kocharov, L. G., Lee, J. W., Zirin, H., et al.: Solar Phys. **155**, 149 (1994) 130
53. Krucker, S., Larson, D. E., Lin, R. P., & Thompson, B. J.: Astrophys. J. **519**, 864 (1999) 130
54. Landau, L. D., & Lifshitz, E. M.: *Fluid Mechanics* (Pergamon, Oxford 1987) 111

55. Lin, R. P., Dennis, B. R., Hurford, G. J., et al.: Solar Phys. **210**, 3 (2002) 130
56. MacQueen, R. M., Blankner, J. G., Elmore, D. F., et al.: Solar Phys. **182**, 97 (1998) 117
57. Mann, G., Aurass, H., Voigt, W., & Paschke, J.: in *Proceedings of the 1st SOHO Workshop: Coronal Streamers, Coronal Loops, and Coronal and Solar Wind Composition*, ESA SP-348, 129 (1992) 120
58. Mann, G.: in *Coronal Magnetic Energy Releases*, eds. A. Benz & A. Krüger (Springer, Berlin 1995a), Lect. Notes Phys. **444**, 183 107
59. Mann, G.: J. Plasma Phys. **53**, 109 (1995b) 111, 121, 132
60. Mann, G., Klassen, A., Classen, H.-T., Aurass, H., Scholz, D., MacDowall, R. J., & Stone, R. G.: Astron. Astrophys. Suppl. **119**, 489 (1996) 119
61. Mann, G., Jansen, F., MacDowall, R. J., et al.: Astron. Astrophys. **348**, 614 (1999a) 108
62. Mann, G., Aurass, H., Klassen, A., et al.: in *Proceedings of the 8th SOHO Workshop: Plasma Dynamics and Diagnostics in the Solar Transition Region and Corona*, ed. B. Kaldeich-Schürmann, ESA SP-446, 477 (1999b) 116, 121, 122, 131
63. Mann, G., Klassen, A., Aurass, H., & Classen, H. T.: Astron. Astrophys. **400**, 329 (2003) 128, 131
64. Melrose, D. B.: Plasma emission mechanisms. In: *Solar Radiophysics*, ed. by McLean, D. J., & Labrum, N. R. (Cambridge Univ. Press, Cambridge 1985), 177 119
65. Moreton, G. E.: Astron. J. **65**, 494 (1960) 108
66. Moreton, G. E., & Ramsey, H. E.: PASP **72**, 357 (1960) 108, 112
67. Moreton, G. E.: Astron. J. **69**, 145 (1964) 108, 112
68. Nakajima, H., Nishio, M., Enome, S., et al.: Proc. IEEE **82**, 705 (1994) 118
69. Nakariakov, V. M., Ofman, L., DeLuca, E., et al.: Science **285**, 862 (1999) 131
70. Narukage, N., Hudson, H. S., Morimoto, T., et al.: Astrophys. J. **572**, L109 (2002) 116, 117, 121, 122
71. Neupert, W. M., Thompson, B. J., Gurman, J. B., & Plunkett, S. P.: J. Geophys. Res. **106**, 25 215 (2001) 129
72. Newkirk, G. A.: Astrophys. J. **133**, 983 (1961) 108
73. Ofman, L., & Thompson, B. J.: Astrophys. J. **574**, 440 (2002) 126
74. Ohyama, M., & Shibata, K.: PASJ **49**, 249 (1997) 127
75. Okamoto, T. J., Nakai, H., Keiyama, A., et al.: Astrophys. J. **608**, 1124 (2004) 114, 115
76. Pearson, D. H., Nelson, R., Kojoian, G., & Seal, J.: Astrophys. J. **336**, 1050 (1989) 128
77. Pizzo, V. J., Hill, S. M., Balch, C. C., et al.: Solar Phys. **226**, 255 (2005) 117
78. Pohjolainen, S., Maia, D., Pick, M., et al.: Astrophys. J. **556**, 421 (2001) 120
79. Priest, E. R.: *Solar Magnetohydrodynamics* (Reidel, Dordrecht 1982) 110, 111
80. Ramsey, H. E., & Smith, S. F.: Astron. J. **71**, 197 (1966) 107, 108
81. Reames, D. V.: Space Sci. Rev. **90**, 413 (1999) 130
82. Reiner, M. J., Kaiser, M. L., Gopalswamy, N., Aurass, H., Mann, G., Vourlidas, A., & Maksimovic, M.: J. Geophys. Res. **106**, 25 279 (2001) 128
83. Roberts, B.: Solar Phys. **193**, 139 (2000) 131
84. Robinson, R. D.: Solar Phys. **95**, 343 (1985) 119
85. Schrijver, C. J., Aschwanden, M. J., & Title, A. M.: Solar Phys. **206**, 69 (2002) 131
86. Shanmugaraju, A., Moon, Y.-J., Dryer, M., & Umapathy, S.: Solar Phys. **215**, 161 (2003) 128

87. Shibata, K., Masuda, S., Shimojo, M., et al.: Astrophys. J. **451**, 83L (1995) 127
88. Smith, S. F., & Harvey, K. L.: in *Physics of the Solar Corona*, ed. C. J. Macris (Reidel, Dordrecht 1971), 156 112, 113, 119, 124
89. Stewart, R. T., McCabe, M. K., Koomen, M. J., Hansen, R. T., & Dulk, G. A.: Solar Phys. **36**, 203 (1974) 127
90. Švestka, Z. & Fritzova-Švestkova, L.: Solar Phys. **36**, 417 (1974) 128
91. Švestka, Z.: *Solar Flares* (Reidel, Dordrecht 1976) 112, 127
92. Thompson, B. J., Plunkett, S. P., Gurman, J. B., et al.: Geophys. Res. Lett. **25**, 2465 (1998) 108, 114, 125
93. Thompson, B. J., Gurman, J. B., Neupert, W. M., et al.: Astrophys. J. **517**, L151 (1999) 114
94. Thompson, B. J., Reynolds, B., Aurass, H., et al.: Solar Phys. **193**, 161 (2000) 114, 126
95. Torsti, J., Anttila, A., Kocharov, L., et al.: Geophys. Res. Lett. **25**, 2525 (1998) 130
96. Torsti, J., Kocharov, L., Teittinen, M., et al.: J. Geophys. Res. **104**, 9903 (1999) 130
97. Tsuneta, S., Acton, L., Bruner, M., et al.: Solar Phys. **136**, 37 (1991) 116
98. Uchida, Y.: PASJ **12**, 376 (1960) 107
99. Uchida, Y.: Solar Phys. **4**, 30 (1968) 108, 116, 132
100. Uchida, Y.: PASJ **22**, 341 (1970) 108, 113
101. Uchida, Y., Altschuler, M. D., & Newkirk, G., Jr.: Solar Phys. **28**, 495 (1973) 108
102. Uchida, Y.: Solar Phys. **39**, 431 (1974) 108
103. Vainio, R., & Khan, J. I.: Astrophys. J. **600**, 451 (2004) 130, 131
104. Valniček, B.: Bull. Astron. Inst. Czech. **15**, 207 (1964) 107
105. Vršnak, B., Ruždjak, V., Zlobec, P., & Aurass, H.: Solar Phys. **158**, 331 (1995) 128
106. Vršnak, B., & Lulić, S.: Solar Phys. **196**, 157 (2000a) 111, 121, 132
107. Vršnak, B., & Lulić, S.: Solar Phys. **196**, 181 (2000b) 127
108. Vršnak, B.: J. Geophys. Res. **106**, 25249 (2001a) 127
109. Vršnak, B.: J. Geophys. Res. **106**, 25291 (2001b) 128
110. Vršnak, B., Aurass, H., Magdalenić, J., & Gopalswamy, N.: Astron. Astrophys. **377**, 321 (2001) 128
111. Vršnak, B., Warmuth, A., Brajša, R., & Hanslmeier, A.: Astron. Astrophys. **394**, 299 (2002a) 117, 118, 120, 124
112. Vršnak, B., Magdalenić, J., Aurass, H., & Mann, G.: Astron. Astrophys. **396**, 673 (2002b)
113. Vršnak, B., Maričić, D., Stanger, A. L., & Veronig, A.: Solar Phys. **225**, 355 (2004) 128
114. Vršnak, B.: Eos, Vol. 86, No. 11, 112 (2005) 133
115. Vršnak, B., Magdalenić, J., Temmer, M., Veronig, A., Warmuth, A., Mann, G., Aurass, H., & Otruba, W.: Astrophys. J. **625**, L67 (2005) 119, 126
116. Wang, Y.-M.: Astrophys. J. **543**, L89 (2000) 121
117. Warmuth, A., Vršnak, B., Aurass, H., & Hanslmeier, A.: Astrophys. J. **560**, L105 (2001) 113, 115
118. Warmuth, A., Vršnak, B., Magdalenić, J., et al.: Astron. Astrophys. **418**, 1101 (2004a) 112, 113, 114, 115, 116, 118, 119, 121, 129
119. Warmuth, A., Vršnak, B., Magdalenić, J., et al.: Astron. Astrophys. **418**, 1117 (2004b) 119, 120, 123

120. Warmuth, A., & Mann, G.: Astron. Astrophys. **435**, 1123 (2005) 116, 120, 121, 122, 132
121. Warmuth, A., & Aurass, H., & Mann, G.: Astrophys. J. **626**, L121 (2005) 117, 121, 128, 12
122. White, S. M., & Thompson, B. J.: Astrophys. J. **620**, L63 (2005) 119, 123
123. Wild, J. P., & McCready, L. L.: Aust. J. Sci. Res. A **3** 387 (1950) 107
124. Wills-Davey, M. J., & Thompson, B. J.: Solar Phys. **190**, 467 (1999) 114, 131
125. Wu, S. T., Zheng, H., Wang, S., et al.: J. Geophys. Res. **106**, 25089 (2001) 121, 122
126. Zarro, D. M., Sterling, A. C., Thompson, B. J, et al.: Astrophys. J. **520**, L139 (1999) 116
127. Zhang, J., Dere, K. P., Howard, R. A., et al.: Astrophys. J. **559**, 452 (2001) 128, 129
128. Zhang, J., Dere, K. P., Howard, R. A., & Vourlidas, A.: Astrophys. J. **604**, 420 (2004) 128
129. Zhukov, A. N., & Auchère, F.: Astron. Astrophys. **427**, 705 (2004) 116
130. Zirin, H., & Russo Lackner, D.: Solar Phys. **6**, 86 (1969) 127